

## Spectroscopic defect imaging in magnetic nanostructure arrays

Han-Jong Chia, Feng Guo, L. M. Belova, and R. D. McMichael

Citation: *Appl. Phys. Lett.* **101**, 042408 (2012); doi: 10.1063/1.4738789

View online: <http://dx.doi.org/10.1063/1.4738789>

View Table of Contents: <http://apl.aip.org/resource/1/APPLAB/v101/i4>

Published by the [American Institute of Physics](#).

---

### Related Articles

Electrical input structures for nanomagnetic logic devices

*J. Appl. Phys.* **111**, 07E341 (2012)

Effects of magnetomechanical vibrations and bending stresses on three-phase three-leg transformers with amorphous cores

*J. Appl. Phys.* **111**, 07E730 (2012)

A novel linear and rotary Halbach permanent magnet actuator with two degrees-of-freedom

*J. Appl. Phys.* **111**, 07E725 (2012)

Improved thrust calculations of active magnetic bearings considering fringing flux

*J. Appl. Phys.* **111**, 07E726 (2012)

Size dependence of spin-torque induced magnetic switching in CoFeB-based perpendicular magnetization tunnel junctions (invited)

*J. Appl. Phys.* **111**, 07C711 (2012)

---

### Additional information on *Appl. Phys. Lett.*

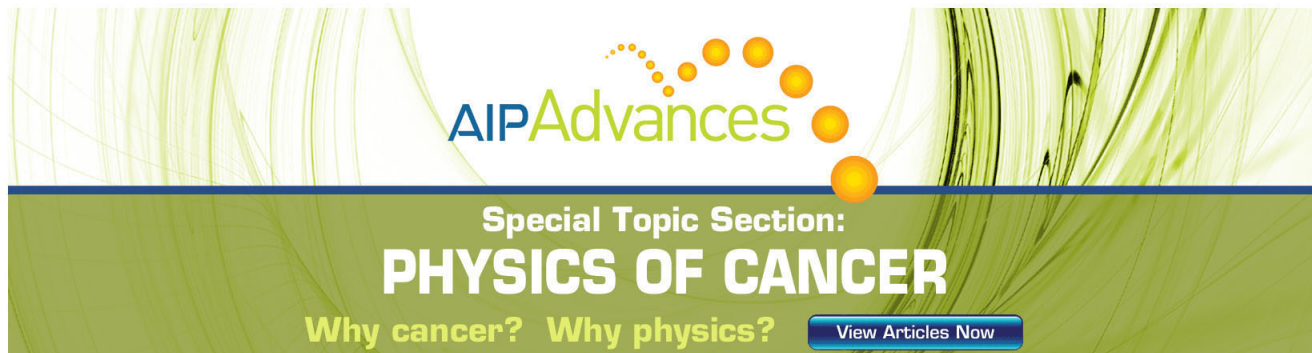
Journal Homepage: <http://apl.aip.org/>

Journal Information: [http://apl.aip.org/about/about\\_the\\_journal](http://apl.aip.org/about/about_the_journal)

Top downloads: [http://apl.aip.org/features/most\\_downloaded](http://apl.aip.org/features/most_downloaded)

Information for Authors: <http://apl.aip.org/authors>

## ADVERTISEMENT

The advertisement features a green and white background with abstract, flowing lines. At the top, the 'AIP Advances' logo is displayed, with 'AIP' in blue and 'Advances' in green, accompanied by a series of orange and yellow dots. Below the logo, the text 'Special Topic Section: PHYSICS OF CANCER' is written in white, with 'PHYSICS OF CANCER' in a larger, bold font. At the bottom, the phrase 'Why cancer? Why physics?' is written in white, and a blue button with the text 'View Articles Now' is positioned on the right side.

AIP Advances

Special Topic Section:  
**PHYSICS OF CANCER**

Why cancer? Why physics? [View Articles Now](#)

## Spectroscopic defect imaging in magnetic nanostructure arrays

Han-Jong Chia,<sup>1,a)</sup> Feng Guo,<sup>1</sup> L. M. Belova,<sup>2</sup> and R. D. McMichael<sup>3,b)</sup>

<sup>1</sup>Center for Nanoscale Science and Technology, National Institute of Standards and Technology, Gaithersburg, Maryland 20899, USA and Maryland Nanocenter, University of Maryland, College Park, Maryland 20742, USA

<sup>2</sup>Department of Materials Science and Engineering, Royal Institute of Technology, 10044 Stockholm, Sweden

<sup>3</sup>Center for Nanoscale Science and Technology, National Institute of Standards and Technology, Gaithersburg, Maryland 20899, USA

(Received 17 February 2012; accepted 9 July 2012; published online 25 July 2012)

We introduce a method for imaging defective structures in an array of magnetic nanodevices using ferromagnetic resonance force microscopy with contrast between normal and defective devices provided through differences in resonance condition. In a demonstration of this technique, two dimensional scans of an array resolve not only intentional differences in resonant field between 200 nm circular dots and an intentional oval “defect,” but also smaller differences between the nominally identical circular dots in the array. © 2012 American Institute of Physics. [<http://dx.doi.org/10.1063/1.4738789>]

The ability to detect and understand sources of defects in arrays of magnetic nanostructures is one of the key criteria in the development of future spintronics technologies. As in existing information technology, future spintronic devices for information processing will likely require large arrays of magnetic nanodevices with highly uniform magnetic properties; limiting defects will be key to manufacturing these arrays with tolerable yields. Minute variations in factors such as shape, damping, and anisotropy between individual bits will dramatically alter the reliability of the device.<sup>1–3</sup> Traditional metrology tools such as scanning electron microscopy (SEM) and atomic force microscopy (AFM) can detect geometrical defects but are blind both to buried devices and magnetic properties.

Much more information can be obtained through spectroscopic techniques such as ferromagnetic resonance (FMR). Ferromagnetic resonance frequencies are sensitive to torques arising from a variety of sources, including magnetocrystalline anisotropy, magnetoelastic effects, sample geometry, spin transfer torques, and interlayer coupling. Additionally, FMR can reveal properties of film edges<sup>4–7</sup> and variations in shape anisotropy.<sup>3</sup> FMR measurements of nanostructures have typically required large arrays of structures to generate a detectable signal.<sup>8–10</sup> In special cases, spectroscopy of single devices can be studied via time-resolved Kerr effect measurements,<sup>11–13</sup> Brillouin light scattering measurements with tightly focused optical spots,<sup>14,15</sup> as well as electrical measurements.<sup>16–19</sup> However, the optical techniques cannot access buried devices and the electrical techniques lack the ability to scan across an array.

Ferromagnetic resonance force microscopy (FMRFM) is a technique that combines the scanned-probe features and buried-device capabilities of magnetic force microscopy (MFM) with the spectroscopic methods of FMR.<sup>20–22</sup> As shown in Fig. 1(a), a magnetic tip is affixed to the end of an AFM-like cantilever. The cantilever is positioned over a sample sitting on a microwave stripline. An external

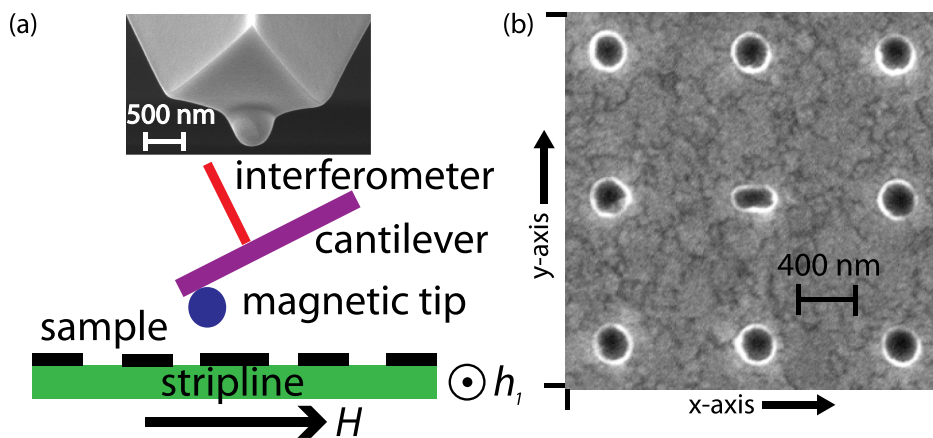
magnetic field  $H$  is applied in the sample plane, aligning the sample magnetization  $M$ . Microwave-frequency current in the stripline generates a microwave field,  $h_1$ , sending the sample spins into precession. Since the magnitude of the magnetization vector is very nearly fixed, precession decreases the quasistatic component of the magnetization, reducing the magnetostatic force between the sample and tip and changing the deflection of the cantilever. The high force sensitivity of the micromechanical cantilever is capable of detecting the small change in magnetization in single nanostructures, and the tip force is optimized by having a magnetic tip with dimensions similar to those of the sample.<sup>7,20</sup> The high spectroscopic resolution of FMR is largely unaffected by mechanical detection except small shifts in the resonance field due to the tip field.

In this letter we describe the use of ferromagnetic resonance force microscopy to image a device array with a defect element using the different dynamic response of the defect element to produce array images with contrast between the defect element and normal elements. We choose a shape defect as a representative case, investigating an oval structure in an array of 200 nm diameter, circular Permalloy dots (Fig. 1(b)).

The sample array was patterned on top of a 10  $\mu\text{m}$  wide, 150 nm thick gold waveguide on silicon with electron beam lithography, followed by electron beam deposition of 5 nm Ta/50 nm Py/5 nm Ta followed by a lift-off. Measurements were performed at 10 GHz at room temperature. Silicon cantilevers with no metallic coating and spring constants of 0.1 N/m were used. The 500 nm diameter cobalt tip was fabricated through electron beam induced deposition (EBID) of cobalt.<sup>23</sup> To enhance detection, the microwave power was modulated at the cantilever frequency. Cantilever motion was detected using the reflectivity of the low-finesse optical cavity formed by the cantilever and the end of an optical fiber. Typical cantilever oscillations were on the order of 20 nm and the tip-sample separation was 150 nm. Cantilever oscillations consist of a resonant component as well as a background contribution that we attribute to microwave heating of the cantilever and sample.

<sup>a)</sup>Electronic mail: hanjong.chia@everspin.com.

<sup>b)</sup>Electronic mail: robert.mcmichael@nist.gov.



We begin discussion of our results with measurements and modeling of individual dots and ovals. One dimensional point spectroscopy scans were done by positioning the tip at different points along lines that cut either through the center axis of the dot or the long axis of the oval and parallel to the external applied field. At each tip position the array was excited at 10.0 GHz and FMR spectra were taken as a function of swept applied field. A linear, non-resonant background was subtracted from each spectrum and the results are shown in Figs. 2(a) and 2(d) for the dot and oval, respectively.

In general, the spectral images of the type shown in Figs 2(a) and 2(d) have a characteristic “arrowhead” shape that includes shifting of the resonance field and a change in sign of the FMRFM signal. The sign change is a feature of the dipolar forces between the tip and the sample.<sup>24,25</sup> When the tip is positioned directly over the center of the sample the cantilever experiences a strong, static, repulsive force. When this force is decreased slightly by the excitation of magnetic resonance, the cantilever deflection yields a positive FMRFM signal, as indicated with the bright area in the center of Fig. 2(a). On the other hand, when the tip is to the left or right of the sample along the field direction, the cantilever experiences an attractive static force, and yields a negative FMRFM signal at resonance. The changing sign of the FMRFM signal is most clearly visible in Fig. 2(a) where the strong, positive signal (light color) in the center of the image is accompanied by weaker, negative signals (black) on the left and right.

The resonance field shift as a function of tip position is an effect of the stray field of the cantilever’s magnetic tip. When the tip is over the sample, the tip field opposes the uniform applied field, and consequently a larger applied field is required to satisfy the resonance conditions of the sample. As the tip is moved away from the sample to the left or right, the tip field weakens and changes sign, and the resonance field moves toward its unperturbed value. The combination of the shifting resonance fields and the varying tip-sample forces produces the arrowhead spectral image shape as the tip is moved across the sample.

A comparison of the spectral images of the disk in Fig. 2(a) and the oval in Fig. 2(d) reveals that the signal from the oval is weaker and that the arrowhead shape is less prominent. The largest effect, however, is the difference between the resonance fields of the dot and oval with the dot

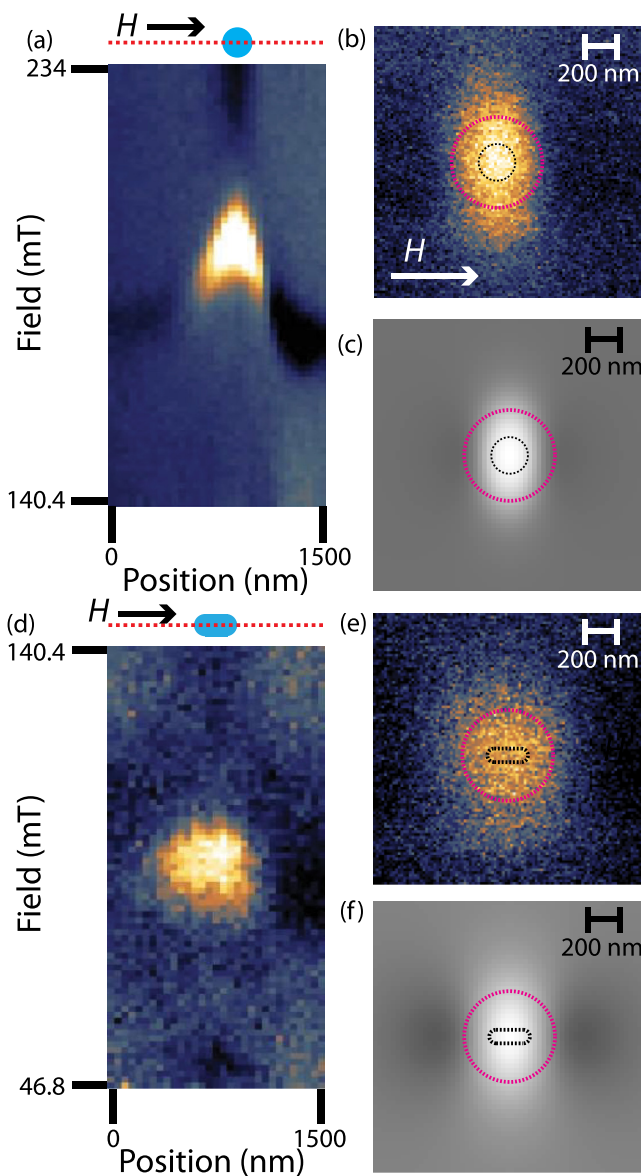


FIG. 2. (a) 1-D point spectroscopy scan across the long axis of the 200 nm dot with an in-plane applied field. The blue dot and red dotted line above indicate the relative size of the dot and the scan direction. (b) FMRFM 2-D scan of an individual 200 nm dot at the dot resonant field. The dotted pink circle denotes the size of the 500 nm tip and the smaller dotted black circle the size of the dot. (c) Micromagnetic simulation of FMRFM 2-D scan of the dot. (d) 1-D point spectroscopy scan along the long axis of the 300 nm  $\times$  150 nm oval defect. (e) 2-D scan of the oval. (f) Micromagnetic simulation of the oval 2-D scan.

resonance at 197 mT and the oval at 95 mT. The difference in shape anisotropy between the circle and the oval produces this large resonance field difference, which also has secondary effects on the measured resonances.

We strongly suspect that the tip magnetization is not saturated in these experiments. The low intensity and the reduced tip field influence in the oval resonance at 95 mT as compared to the disk resonance at 197 mT are both consistent with an unsaturated tip magnetization. Further, the tip field estimated for a saturated cobalt tip is approximately 140 mT, which is quite large compared to the 20 mT scale of the field perturbations evident in the arrowhead of Fig. 2(a). The assumption of an unsaturated tip of ideally soft material yields a more reasonable tip field estimate of 50 mT at the applied field of 200 mT.

We then set the external field to that the resonant fields of the dot and oval and perform a two dimensional  $1.5 \mu\text{m} \times 1.5 \mu\text{m}$  scan of each (Figs. 2(b) and 2(e)). The scan size is  $100 \times 100$  pixels with 100 ms averaging per point. The pink dotted circle denotes the superimposed size of the 500 nm tip and the smaller black dotted circle denotes the size of the sample. For both the oval and dot we see elongated FMRFM images with the short axis parallel to the applied field. To the left and right of the main signal, there are darker regions corresponding to the dark regions in the 1-D point spectroscopy scan. The spatial size of the detected signal is roughly the size of the tip since the resolution of our scans is roughly equal to the size of the tip, at small tip-sample separations. Thus, our observed signal is much larger than the actual size of the sample, which is also evident in the 1-D point spectroscopy measurement and gives us a rough resolution of 500 nm.

To interpret our 2-D scans we performed micromagnetic modeling through the object oriented micromagnetic framework (OOMMF)<sup>26</sup> to generate modeled FMRFM 2-D scans (Fig. 2(c) and 2(f)). For each tip position, the dynamic response to a short field pulse is calculated in the presence of a uniform applied field  $H$  and a nonuniform component due to the magnetic tip. The tip is modeled as a 500 nm diameter sphere of perfectly soft material so that  $M = 3H$ . For each cell of the micromagnetic simulation, we calculate the reduction in static magnetization  $\Delta M_x(x, y, f)$  and the corresponding change in the dipolar force between the micromagnetic cell and the tip. Finally, the force contributions are summed over the cells to yield a simulated FMRFM signal. The modeled responses are similar in form to the experimental results, and in particular we note the elongated shape of the image and the rough equivalence of the tip size and the image size.

With the resonance data from the individual elements to serve as a guide, we performed a one dimensional point spectroscopy scan on the array, scanning first along a line connecting two dots with an oval between them (Fig. 3(a)). The resonances of the dots at high field are distinctly different from the oval resonance at low field. Additionally, there are subtler but clear differences between the resonances of the nominally identical dots in this line scan. From the data in the 1-D point spectroscopy measurement we then set the applied field to the resonance field of either the oval or the left dot and perform a  $3.9 \mu\text{m} \times 3.9 \mu\text{m}$  scan of the array.

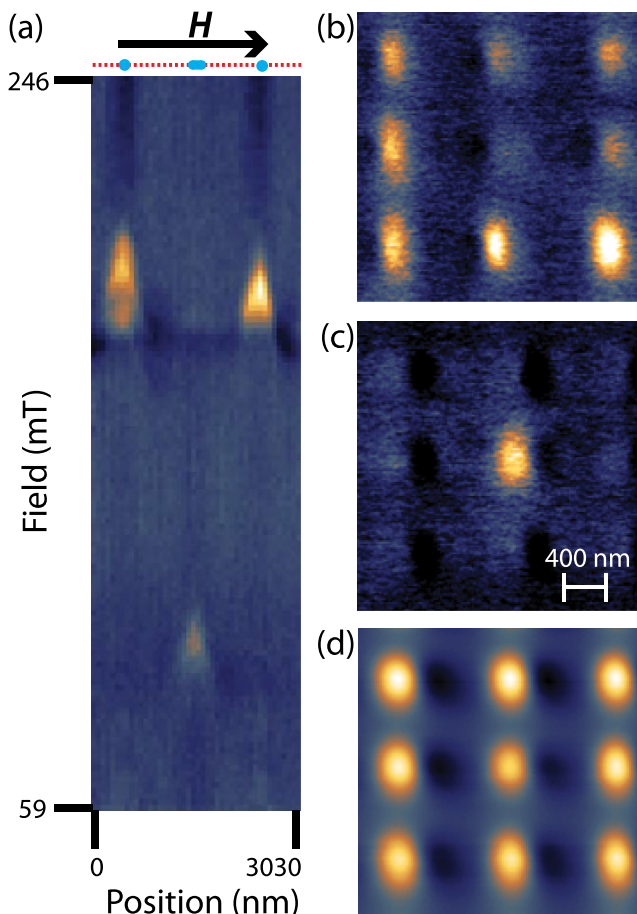


FIG. 3. (a) 1-D point spectroscopy scan across 2 dots and an oval. The dotted red line on the top indicates the scan direction. (b) 2-D FMRFM scan set at an applied field of 197 mT, the resonance field of one of the dots. The oval defect does not resonate at this field and the magnitude of several of the other dots is weaker since they have slightly different resonant fields. (c) 2-D FMRFM scan set at 95 mT, the resonance field of the oval. Only the oval defect is visible. (d) Magnetic force microscopy (MFM) scan taken simultaneously with the FMRFM scans. The dots appear fairly uniform and the oval yields a slightly spatially smaller signal.

In Fig. 3(b) with the field set at a dot's resonance field, the scan reveals resonances in all the dots in the array but the oval's resonance image is very faint. Fig. 3(a) shows that the dots to the left and right of the oval have slightly different resonance fields and in the 2D scan; these differences produce different image intensities in these two dots, as well as the others in the array. In Fig. 3(c) we set the applied field to that of the oval and the 2D image shows resonance only at the oval. For comparison, in Fig. 3(d) we show a magnetic force microscopy (MFM) scan taken simultaneously with the FMRFM scans (the frequency shift signal from the PLL). The MFM image shows little difference between the dots and the oval.

The spectroscopic sensitivity and scanned probe capabilities of FMRFM suggest development of the method for a wafer level metrology tool. Looking ahead on that path, we conclude this paper with speculation on the sensitivity, and field resolution challenges facing development of such a tool for measurement of magnetic memory cells or other nanomagnetic devices.

To measure thinner films in smaller devices, the tip force will be important. The signal to noise ratio (SNR) of

the 200 nm diameter, 50 nm thick disks in this study is on the order of 20 with 1 s integration time. To scale these results, we derive a simple model for the force between a spherical tip with radius  $a$ , and a thin, disk-shaped sample of radius  $b$  and thickness  $t$ . Both the tip and sample are assumed to be magnetized in the  $x$ -direction. The tip-sample interaction energy for a tip lifted a distance  $h$  above the sample is

$$E_{\text{tip-disk}} = -\mu_0 \int_V dv \mathbf{H}_{\text{tip}}(h) \cdot \mathbf{M}_{\text{sample}}, \quad (1)$$

where  $\mathbf{H}_{\text{tip}}$  is the dipole field of the spherical tip. A derivative of Eq. (1) with respect to  $h$  yields the tip-sample force, and finally, the resonance-induced change in the force  $\Delta F_{\text{tip}}$  is obtained by replacing  $\mathbf{M}_{\text{sample}}$  with the resonance-induced magnetization change in the sample,  $\Delta M$ .

$$\Delta F_{\text{tip}} \approx \mu_0 M_{\text{tip}} \Delta M \frac{a^3 \pi b^2 t (a + h + t/2)}{[b^2 + (a + h + t/2)^2]^{5/2}}, \quad (2)$$

where  $M_{\text{tip}}$  is the tip magnetization. Using Eq. (2), we project that for a 100 nm diameter, 4 nm thick sample disk, a SNR of 2.5 will be attainable with a 300 nm diameter tip and 30 nm tip-sample separation. Compensating improvements in SNR may be expected by using a fully saturated tip moment.

The field resolution of the measurement in terms of the ability to measure resonance peak shifts depends on the slope of a resonance peak and the measurement noise level. We define the field resolution as the minimum field shift that produces a signal change that is greater than the noise level. For a resonance shift  $\delta H$  of a Lorentzian resonance peak, the greatest signal change occurs on the sides of the peak, at the points with maximum slope. Setting the signal change due to a field shift  $\delta H$  at this point to the noise level, we obtain

$$\delta H \geq \frac{4}{3\sqrt{3}} \frac{\Delta H}{\text{SNR}}, \quad (3)$$

where  $\Delta H$  is the full-width at half-maximum line width of the resonance peak, SNR is the signal to noise ratio at the resonance maximum<sup>27</sup> and the numerical pre-factor is particular to a Lorentzian line shape. For a material with damping parameter  $\alpha = 0.01$  and  $\text{SNR} = 20$ , this estimate suggests a field resolution of 0.2 mT (2 Oe) in the current measurements.

In summary, this paper demonstrates a method for magnetic defect imaging through ferromagnetic resonance force microscopy. The ferromagnetic resonance spectra of magnetic nanostructures provide the image contrast with field resolution on the order of  $10^{-4}$  T. Scaling to smaller sample sizes appears feasible, but depends on the details of the tip and sample geometries.

We are grateful for valuable discussions with E. D. Dahlberg and Konrad Aschenbach, H. Chia, and F. Guo acknowledge support under the Cooperative Research Agreement between the University of Maryland and the National Institute of Standards and Technology Center for Nanoscale Science and Technology, Award 70NANB10H193, through the University of Maryland.

<sup>1</sup>Y. Katoh, S. Saito, H. Honjo, R. Nebashi, N. Sakimura, T. Suzuki, S. Miura, and T. Sugibayashi, *IEEE Trans. Magn.* **45**, 3804 (2009).

<sup>2</sup>J. Slaughter, *Annu. Rev. Mater. Res.* **39**, 277 (2009).

<sup>3</sup>H. T. Nembach, J. M. Shaw, T. J. Silva, W. L. Johnson, S. A. Kim, R. D. McMichael, and P. Kabos, *Phys. Rev. B* **83**, 094427 (2011).

<sup>4</sup>R. D. McMichael and B. B. Maranville, *Phys. Rev. B* **74**, 024424 (2006).

<sup>5</sup>M. Zhu and R. D. McMichael, *J. Appl. Phys.* **107**, 103908 (2010).

<sup>6</sup>B. B. Maranville, R. D. McMichael, and D. W. Abraham, *Appl. Phys. Lett.* **90**, 232504 (2007).

<sup>7</sup>H.-J. Chia, F. Guo, L. M. Belova, and R. D. McMichael, "Two dimensional spectroscopic imaging of individual ferromagnetic nanostripes" (unpublished).

<sup>8</sup>M. Pechan, C. Yu, D. Owen, J. Katine, L. Folks, and M. Carey, *J. Appl. Phys.* **99**, 08C702 (2006).

<sup>9</sup>J. Shaw, T. Silva, M. Schneider, and R. McMichael, *Phys. Rev. B* **79**, 184404 (2009).

<sup>10</sup>G. Gubbiotti, G. Carlotti, T. Okuno, M. Grimsditch, L. Giovannini, F. Montoncello, and F. Nizzoli, *Phys. Rev. B* **72**, 184419 (2005).

<sup>11</sup>P. Keatley, V. Kruglyak, A. Neudert, M. Delchini, R. Hicken, J. Childress, and J. Katine, *J. Appl. Phys.* **105**, 07D308 (2009).

<sup>12</sup>M. Belov, Z. Liu, R. D. Sydora, and M. R. Freeman, *Phys. Rev. B* **69**, 094414 (2004).

<sup>13</sup>Z. Liu, R. Brandt, Y. Yahagi, B. Hansen, B. Harteneck, J. Bokor, A. R. Hawkins, and H. Schmidt, *Appl. Phys. Lett.* **98**, 052502 (2011).

<sup>14</sup>S. O. Demokritov and E. Demidov, *Vladislav, IEEE Trans. Magn.* **4**, 6 (2008).

<sup>15</sup>V. E. Demidov, M. Buchmeier, K. Rott, P. Krzysteczko, J. Munchenberger, G. Reiss, and S. O. Demokritov, *Phys. Rev. Lett.* **104**, 217203 (2010).

<sup>16</sup>J. Sankey, P. Braganca, A. G. Garcia, I. Krivorotov, R. Buhrman, and D. Ralph, *Phys. Rev. Lett.* **96**, 227601 (2006).

<sup>17</sup>G. Fuchs, J. Sankey, V. Pribiag, L. Qian, P. Braganca, A. Garcia, E. Ryan, Z.-P. Li, O. Ozatay, D. Ralph *et al.*, *Appl. Phys. Lett.* **91**, 062507 (2007).

<sup>18</sup>J. C. Sankey, Y.-T. Cui, J. Z. Sun, J. C. Slonczewski, R. A. Buhrman, and D. C. Ralph, *Nat. Phys.* **4**, 67 (2008).

<sup>19</sup>H. Kubota, A. Fukushima, K. Yakushiji, T. Nagahama, S. Yuasa, K. Ando, H. Maehara, Y. Nagamine, K. Tsunekawa, D. D. Djayaprawira *et al.*, *Nat. Phys.* **4**, 37 (2008).

<sup>20</sup>O. Klein, G. de Loubens, V. Naletov, F. Boust, T. Guillet, H. Hurdenquint, A. Leksikov, A. Slavin, V. Tiberkevich, and N. Vukadinovic, *Phys. Rev. B* **78**, 144410 (2008).

<sup>21</sup>Z. Zhang, P. C. Hammel, and P. E. Wigen, *Appl. Phys. Lett.* **68**, 2005 (1996).

<sup>22</sup>T. Mewes, J. Kim, D. V. Pelekhov, G. N. Kakazei, P. E. Wigen, S. Batra, and P. C. Hammel, *Phys. Rev. B* **74**, 144424 (2006).

<sup>23</sup>L. M. Belova, E. D. Dahlberg, A. Riazanova, J. J. L. Mulders, C. Christophersen, and J. Eckert, *Nanotechnology* **22**, 145305 (2011).

<sup>24</sup>Y. Obukhov, D. V. Pelekhov, J. Kim, P. Banerjee, I. Martin, E. Nazaretski, R. Movshovich, S. An, T. J. Gramila, S. Batra *et al.*, *Phys. Rev. Lett.* **100**, 197601 (2008).

<sup>25</sup>H.-J. Chia, F. Guo, L. M. Belova, and R. D. McMichael, *Phys. Rev. Lett.* **108**, 087206 (2012).

<sup>26</sup>M. J. Donahue and D. G. Porter, *OOMMF User's Guide, Version 1.0*, (National Institute of Standards and Technology, Gaithersburg, MD, September 1999).

<sup>27</sup>I. Lee, Y. Obukhov, G. Xiang, A. Hauser, F. Yang, P. Banerjee, D. Pelekhov, and P. Hammel, *Nature* **466**(Suppl.), 845 (2010).